Defence Research and Development Canada
Recherche et développement pour la défense Canada

CAN UNCLASSIFIED

DRDC | RDDC
technologysciencetechnologie

Satellite launcher navigation aided by a stochastic model of the vehicle

Yanick Beaudoin
André Desbiens
Département de génie électrique et de génie informatique, Université Laval

Eric Gagnon
Defence Research and Development Canada

René Jr. Landry
Département de génie électrique, École de technologies Supérieure

18th Astronautics Conference (ASTRO 2018)
Québec City, Canada, May 15-17 2018

Date of Publication from Ext Publisher: June 2018

Defence Research and Development Canada
External Literature (N)
DRDC-RDDC-2018-N095
July 2018

Canada

IMPORTANT INFORMATIVE STATEMENTS

This document was reviewed for Controlled Goods by Defence Research and Development Canada using the Schedule to the *Defence Production Act*.

Satellite launcher navigation aided by a stochastic model of the vehicle

Yanick Beaudoin[1], André Desbiens[1], Eric Gagnon[2], and René Jr. Landry[3]

[1]Département de génie électrique et de génie informatique, Université Laval, 1065 avenue de la Médecine, Québec city, Québec, Canada
[2]Defence Research and Development Canada, 2459 Route de la Bravoure, Québec city, Québec, Canada
[3]Département de génie électrique, École de technologies Supérieure, 1100 Rue Notre-Dame Ouest, Montréal, Québec, Canada

Abstract

The navigation system of a satellite launcher is of paramount importance. On a small launcher targeting low orbit, the navigation system may be a significant part of the total mission cost. A trend which is gaining interest is exploiting a model of the vehicle dynamics into the navigation system. Navigation with vehicle dynamics was evaluated on ground vehicles, aircrafts and unmanned helicopters/quadricopters. However, to the knowledge of the authors, navigation aided by the model of the dynamics has not been tested for satellite launchers.

Adding the vehicle dynamics knowledge into the navigation system can be as simple as adding nonholonomicity constraints or it may need a complete model of the vehicle dynamics. In this paper, a simple stochastic model that represents the angular velocity and acceleration as random walks with known driving noise variances, which are based on the vehicle dynamics, is exploited. The estimated values are then updated with the gyroscope and accelerometer measurements.

The results show that the attitude, velocity and position estimates are barely improved. However, the angular velocity and acceleration estimation errors are reduced significantly. Also, the proposed solution does not require special maneuvers to ensure the observability of the navigation model. To illustrate the advantage of the proposed approach, the improved angular velocity estimates are exploited in the control function instead of the raw gyroscope measurements to significantly reduce thrust nozzle movements.

Notation

Latines letters

0_i	$i \times i$ zero matrix
A	state matrix
a_e	acceleration estimation
$\boldsymbol{a_e^B}$	acceleration estimation
a_m	acceleration measurement
$\boldsymbol{a_m^B}$	acceleretion measurement
b_a	accelerometer bias
$\boldsymbol{b_a^B}$	accelerometer bias
$\boldsymbol{b_g^B}$	gyroscope bias
B_m	measurement input matrix
$\boldsymbol{b_p^E}$	GPS position bias

B_s stochastic value input matrix

c_a accelerometer bias Markov process time constant

c_g gyroscope bias Markov process time constant

c_p GPS position bias Markov process time constant

I_i $i \times i$ identity matrix

k time step

Q state covariance matrix

Q_1 state covariance matrix

Q_s stochastic value covariance matrix

R observation covariance matrix

R_1 observation covariance matrix

s_t sampling time

$\mathbf{T_B^E}$ rotation matrix from the body frame to the Earth frame

$\boldsymbol{u_m}$ measurement input vector

$\boldsymbol{u_s}$ stochastic value input vector

$\boldsymbol{x}$ state vector

Greek letters

$[\alpha_{c\psi}]_{IB}^{B}$ commanded yaw angular acceleration

$[\alpha_{c\theta}]_{IB}^{B}$ commanded pitch angular acceleration

$\boldsymbol{[\alpha_e]_{IB}^{B}}$ angular acceleration estimation

$[\alpha_{e\phi}]_{IB}^{B}$ modelled roll angular acceleration amplitude

$[\alpha_{e\psi}]_{IB}^{B}$ modelled yaw angular acceleration amplitude

$[\alpha_{e\theta}]_{IB}^{B}$ modelled pitch angular acceleration amplitude

Δa_e jerk estimation

$\boldsymbol{\Delta a_e^B}$ jerk estimation

$\Delta {a_e}_x^B$ modelled x-axis jerk amplitude

$\Delta {a_e}_y^B$ modelled y-axis jerk amplitude

$\Delta {a_e}_z^B$ modelled z-axis jerk amplitude

Δa_m acceleration measurement noise (random walk)

$\boldsymbol{\Delta a_m^B}$ accelerometer measurement noise (random walk)

Δb_a accelerometer bias Markov process driving noise

$\boldsymbol{\Delta b_a^B}$ accelerometer bias Markov process driving noise

$\boldsymbol{\Delta b_g^B}$ gyroscope bias Markov process driving noise

$\boldsymbol{\Delta b_p^E}$ GPS position bias Markov process driving noise

$\boldsymbol{[\Delta \omega_m]_{IB}^{B}}$ gyroscope measurement noise (random walk)

$\boldsymbol{\delta \Psi_e^E}$ attitude estimation error

$\boldsymbol{\Delta \Psi_m^E}$ attitude measurement noise

$\boldsymbol{\delta \Psi_m^E}$ attitude estimation error measurement

$\boldsymbol{\delta r_e^E}$ position estimation error

$\boldsymbol{\Delta r_m^E}$ position measurement noise

$\boldsymbol{\delta r_m^E}$ position estimation error measurement

δv_e velocity estimation error

$\boldsymbol{\delta v_e^E}$ velocity estimation error

Δv_m velocity measurement noise

δv_m velocity estimation error measurement

$\boldsymbol{\Delta v_m^E}$ velocity measurement noise

$\boldsymbol{\delta v_m^E}$ velocity estimation error measurement

$\Delta \xi_{c\psi}^B$ variations of the commanded thrust nozzle angle to correct the yaw of the launcher

$\Delta \xi_{c\theta}^B$ variations of the commanded thrust nozzle angle to correct the pitch of the launcher

$[\boldsymbol{\omega_e}]_{\boldsymbol{IB}}^{\boldsymbol{B}}$ angular velocity estimation

$\boldsymbol{\omega_{IE}^E}$ angular velocity of the Earth rotation

$[\boldsymbol{\omega_m}]_{\boldsymbol{IB}}^{\boldsymbol{B}}$ angular velocity measurement

Subscripts and superscripts

$\{\cdot\}^B$ variable represented in the body frame

$\{\cdot\}^E$ variable represented in the Earth frame

1 Introduction

For a satellite launcher, the navigation is of paramount importance. On a small launcher targeting low orbit, the cost of the navigation system may take significant proportions [1]. Therefore, the best uses of the available information must be done. A trend which is gaining interest is exploiting the knowledge of the vehicle dynamics. But, to the knowledge of the authors, this approach has never been studied for a satellite launchers. The Ariane 5 navigation system employs a ballistic trajectory during its coast phase, where the sensor measurements are not used, and the boost phases rely solely on sensor data [2]. In this paper, a stochastic launcher model is combined with sensor measurements to improve navigation performances.

The use of the vehicle dynamics is suggested by Koifman and Bar-Itzhack [3] in a feasibility analysis for an aircraft. The results show that the position and roll estimation errors are greatly reduced and that a constant wind speed can be estimated. However, some maneuvers are needed to ensure observability. Without those maneuvers, the filter diverges and the inclusion of the aircraft dynamics becomes useless [3, 4, 5]. Motions, such as Dutch roll, are critical to excite the coupling of errors in the flight vehicle model [6]. For efficiency reasons, the trajectory of a satellite launcher is smooth and doing those maneuvers would be a waste of energy.

Unlike the previous approaches where the IMU is used as the prime navigation sensor aided by the vehicle model, Khaghani and Skaloud [7] suggest to employ the vehicle dynamics model to propagate the navigation states and correct estimates with sensor data. This architecture is less sensitive to sensor failures since it can stop using defective sensors. But the model is complex in a simulation context for a UAV and the implementation in a real scenario is expected to be challenging due to unmodelled dynamics and disturbances [7].

The vehicle dynamics aided navigation was also tested on a small scale helicopter to reduce the impact of sensor failures [8]. But, despite a complex model, the velocity and position errors grow rapidly during GPS outages [9]. Also, the observability of the model is not guaranteed unless some maneuvers are performed [9]. For a quadricopter, the drag force introduces a stabilizing term which is an essential source for the increased performance (i.e. the speed of the quadricopter cannot be infinite) [9]. However, for a satellite launcher, the drag force becomes almost null during the exoatmospheric phase.

On ground vehicles, non-holonomic constraints can be exploited [4, 10, 11, 12]. Based on the fact that the lateral and vertical velocities are almost null, virtual velocity observations are added to the navigation model as soft constrains [13]. The use of constraints solely does not provide full observability [4] and, as with aerial vehicles, some maneuvers are needed to ensure a complete observability [4, 11]. The exploitation of constraints reduces the error growth between GPS measurements, which increase the GPS denied navigation capabilities [4]. When combined with an axial velocity encoder, the a priori knowledge of the vehicle dynamics can drastically improve the navigation performances [4, 11]. But this approach is not purely based on the vehicle dynamics and part of the gain should be attributed to the additional sensor. Unlike ground vehicles, satellite launchers are holonomic (i.e launchers can move in all directions). However, they are under actuated which prevents fast angular rate and lateral acceleration maneuvers [14].

A simple heuristic model of the dynamics was tested on a gun launched projectile and demonstrated good improvement on the position estimation [15]. However, the dynamics of a launcher is complex and vary a lot during a mission, which prevents the use of a simple model.

A complex vehicle model may lead to model errors, over-parameterization of the model and poor observability, which may degrade the performance of the navigation filter [10, 16]. In some cases, the unobservability problem can be compensated with the use of weak constraints [16]. On the other side, simple stochastic models are already exploited with success to model sensor imperfections [17, 18, 19]. The stochastic model of the sensor errors can be further improved by taking into account the dynamics of the vehicle [20]. The modelling of the angular velocity as a random walk, updated with gyroscope measurements, has already been done [21]. However, it was exploited as a means of combining gyroscopes in an array and not as a way to include the vehicle dynamics knowledge into the navigation system.

For a satellite launcher, the angular velocity and acceleration vary slowly for most of the time during the mission. The exceptions are stage changes and turn maneuvers which are predictable since commanded. The first contribution of this paper is to demonstrate that this knowledge can be exploited in a simple stochastic model, added to a baseline navigation system, to improve the angular velocity and acceleration estimates (section 2). Furthermore, this approach does not introduce unobservability problems as many aforementioned solutions. The second contribution of this paper is to show that the improved angular velocity estimation can be exploited to refine the control function of the launcher and thus reduce the movement of the thrust nozzle (section 3).

2 Navigation with vehicle dynamics

In order to include the knowledge of the launcher dynamics, the loosely coupled GPS/INS aided by a reference attitude sensor (e.g. magnetometer) is augmented to include the angular velocity and acceleration estimates. The angular velocity and acceleration are modelled as random walks with known driving noise variances, which are based on the knowledge of the angular acceleration and jerk that can be undergone by the launcher. Then, the angular velocity and acceleration estimates are updated using the gyroscope and accelerometer measurements. Section 2.1 shows how the acceleration estimation can be implemented in a simplified, one dimension, error state model. In section 2.2, the principle is applied to the complete error state model to include the angular velocity and acceleration. The models, exploited to adjust the navigation filter angular acceleration and jerk variances according to the launcher dynamics, are presented in section 2.3. The navigation performances are analyzed in section 2.4.

2.1 Acceleration estimation

This section shows how the acceleration estimation can be integrated in a simplified, one dimension model, which includes only the accelerometer bias and velocity estimation error. For this model, the only measurements available are the acceleration and velocity.

The acceleration estimation a_e from time step k to time step $k+1$ is:

$$a_{e(k+1)} = a_{e(k)} + s_t \Delta a_{e(k)} \tag{1}$$

where Δa_e is the estimated jerk and s_t is the sampling time. The acceleration measurement a_m is the

acceleration estimation plus the accelerometer bias b_a and random walk noise Δa_m:

$$a_{m(k)} = a_{e(k)} + b_{a(k)} + \Delta a_{m(k)} \tag{2}$$

The time evolution of the velocity estimation error δv_e is:

$$\delta v_{e(k+1)} = \delta v_{e(k)} + s_t \left(a_{m(k)} - a_{e(k)} \right) \tag{3}$$

and the time evolution of the estimated bias is:

$$b_{a(k+1)} = b_{a(k)} + s_t \Delta b_{a(k)} \tag{4}$$

where Δb_a is the variation of the accelerometer bias estimation. The measured velocity estimation error $\delta v_{m(k)}$ is the velocity estimation error plus the velocity measurement noise Δv_m:

$$\delta v_{m(k)} = \delta v_{e(k)} + \Delta v_{m(k)} \tag{5}$$

Grouping (1), (2), (3), (4) and (5) into a matrix form gives the following state representation:

$$\begin{bmatrix} a_{e(k+1)} \\ b_{a(k+1)} \\ \delta v_{e(k+1)} \end{bmatrix} = \left[I_3 + s_t \begin{bmatrix} 0 & 0 & 0 \\ 0 & 0 & 0 \\ -1 & 0 & 0 \end{bmatrix} \right] \begin{bmatrix} a_{e(k)} \\ b_{a(k)} \\ \delta v_{e(k)} \end{bmatrix} + s_t \begin{bmatrix} 0 \\ 0 \\ a_{m(k)} \end{bmatrix} + s_t \begin{bmatrix} \Delta a_{e(k)} \\ \Delta b_{a(k)} \\ 0 \end{bmatrix}$$

$$\begin{bmatrix} a_{m(k)} \\ \delta v_{m(k)} \end{bmatrix} = \begin{bmatrix} 1 & 1 & 0 \\ 0 & 0 & 1 \end{bmatrix} \begin{bmatrix} a_{e(k)} \\ b_{a(k)} \\ \delta v_{e(k)} \end{bmatrix} + \begin{bmatrix} \Delta a_{m(k)} \\ \Delta v_{m(k)} \end{bmatrix}$$

where I_i is a $i \times i$ identity matrix. The corresponding state covariance matrix Q_1 and observation covariance matrix R_1 are:

$$Q_{1(k)} = \begin{bmatrix} E\left[\Delta a_{e(k)} \Delta a_{e(k)}^T\right] & 0 & 0 \\ 0 & E\left[\Delta b_{a(k)} \Delta b_{a(k)}^T\right] & 0 \\ 0 & 0 & 0 \end{bmatrix}$$

$$R_{1(k)} = \begin{bmatrix} E\left[\Delta a_{m(k)} \Delta a_{m(k)}^T\right] & 0 \\ 0 & E\left[\Delta v_{m(k)} \Delta v_{m(k)}^T\right] \end{bmatrix}$$

where $E[\cdot]$ is the mathematical expectation.

If the jerk of the launcher is completely unknown (i.e. $E\left[\Delta a_e \Delta a_e{}^T\right] = \infty$), the acceleration estimation relies almost solely on the accelerometer measurements, as it will be shown in section 2.4.2. The same mathematical developpement can be done for the augular velocity by replacing the acceleration, velocity, etc. by their equivalents in rotational dynamics.

2.2 Implementation into the complete error state model

The baseline navigation system is a loosely coupled GPS/INS with attitude reference sensors, where the error state model includes the attitude $\boldsymbol{\delta\Psi_e^E}$, velocity $\boldsymbol{\delta v_e^E}$ and position $\boldsymbol{\delta r_e^E}$ estimation errors. The estimations of the gyroscope $\boldsymbol{b_g^B}$, accelerometer $\boldsymbol{b_a^B}$ and GPS position $\boldsymbol{b_p^E}$ biases are represented by Markov processes with corresponding time constants (c_g, c_a, c_p) and driving noises ($\boldsymbol{\Delta b_g^B}$, $\boldsymbol{\Delta b_a^B}$, $\boldsymbol{\Delta b_p^E}$). The measured estimation errors of the attitude $\boldsymbol{\delta\Psi_m^E}$, velocity $\boldsymbol{\delta v_m^E}$ and position $\boldsymbol{\delta r_m^E}$ are affected by corresponding measurement noises ($\boldsymbol{\Delta\Psi_m^E}$, $\boldsymbol{\Delta v_m^E}$, $\boldsymbol{\Delta r_m^E}$).

Adding the angular velocity $[\boldsymbol{\omega_e}]^{\boldsymbol{B}}_{\boldsymbol{IB}}$ and acceleration $\boldsymbol{a}^{\boldsymbol{B}}_{\boldsymbol{e}}$ estimations to the baseline navigation system gives the following model:

$$
\begin{bmatrix}
[\boldsymbol{\omega_e}]^{\boldsymbol{B}}_{\boldsymbol{IB}\,(k+1)} \\
\boldsymbol{a}^{\boldsymbol{B}}_{\boldsymbol{e}\,(k+1)} \\
\boldsymbol{\delta\Psi}^{\boldsymbol{E}}_{\boldsymbol{e}\,(k+1)} \\
\boldsymbol{\delta v}^{\boldsymbol{E}}_{\boldsymbol{e}\,(k+1)} \\
\boldsymbol{\delta r}^{\boldsymbol{E}}_{\boldsymbol{e}\,(k+1)} \\
\boldsymbol{b}^{\boldsymbol{B}}_{\boldsymbol{g}\,(k+1)} \\
\boldsymbol{b}^{\boldsymbol{B}}_{\boldsymbol{a}\,(k+1)} \\
\boldsymbol{b}^{\boldsymbol{E}}_{\boldsymbol{p}\,(k+1)}
\end{bmatrix}
=
\begin{bmatrix}
I_{24} + s_t \begin{bmatrix}
0_3 & 0_3 & 0_3 & 0_3 & 0_3 & 0_3 & 0_3 & 0_3 \\
0_3 & 0_3 & 0_3 & 0_3 & 0_3 & 0_3 & 0_3 & 0_3 \\
\mathbf{T}^{\mathbf{E}}_{\mathbf{B}\,(k)} & 0_3 & -\boldsymbol{\omega}^{\boldsymbol{E}}_{\boldsymbol{IE}}\times & 0_3 & 0_3 & 0_3 & 0_3 & 0_3 \\
0_3 & -\mathbf{T}^{\mathbf{E}}_{\mathbf{B}\,(k)} & \left(\mathbf{T}^{\mathbf{E}}_{\mathbf{B}\,(k)}\boldsymbol{a}^{\boldsymbol{B}}_{\boldsymbol{m}\,(k)}\right)\times & -2\boldsymbol{\omega}^{\boldsymbol{E}}_{\boldsymbol{IE}}\times & 0_3 & 0_3 & 0_3 & 0_3 \\
0_3 & 0_3 & 0_3 & I_3 & 0_3 & 0_3 & 0_3 & 0_3 \\
0_3 & 0_3 & 0_3 & 0_3 & 0_3 & -\frac{1}{c_g}I_3 & 0_3 & 0_3 \\
0_3 & 0_3 & 0_3 & 0_3 & 0_3 & 0_3 & -\frac{1}{c_a}I_3 & 0_3 \\
0_3 & 0_3 & 0_3 & 0_3 & 0_3 & 0_3 & 0_3 & -\frac{1}{c_p}I_3
\end{bmatrix}
\end{bmatrix}
\begin{bmatrix}
[\boldsymbol{\omega_e}]^{\boldsymbol{B}}_{\boldsymbol{IB}\,(k)} \\
\boldsymbol{a}^{\boldsymbol{B}}_{\boldsymbol{e}\,(k)} \\
\boldsymbol{\delta\Psi}^{\boldsymbol{E}}_{\boldsymbol{e}\,(k)} \\
\boldsymbol{\delta v}^{\boldsymbol{E}}_{\boldsymbol{e}\,(k)} \\
\boldsymbol{\delta r}^{\boldsymbol{E}}_{\boldsymbol{e}\,(k)} \\
\boldsymbol{b}^{\boldsymbol{B}}_{\boldsymbol{g}\,(k)} \\
\boldsymbol{b}^{\boldsymbol{B}}_{\boldsymbol{a}\,(k)} \\
\boldsymbol{b}^{\boldsymbol{E}}_{\boldsymbol{p}\,(k)}
\end{bmatrix}
\\
\underbrace{+ s_t \begin{bmatrix}
0_3 & 0_3 \\
0_3 & 0_3 \\
-\mathbf{T}^{\mathbf{E}}_{\mathbf{B}\,(k)} & 0_3 \\
0_3 & \mathbf{T}^{\mathbf{E}}_{\mathbf{B}\,(k)} \\
0_3 & 0_3 \\
0_3 & 0_3 \\
0_3 & 0_3 \\
0_3 & 0_3
\end{bmatrix}
\begin{bmatrix}
[\boldsymbol{\omega_m}]^{\boldsymbol{B}}_{\boldsymbol{IB}\,(k)} \\
\boldsymbol{a}^{\boldsymbol{B}}_{\boldsymbol{m}\,(k)}
\end{bmatrix}}_{\text{measurements}}
+
\underbrace{s_t \begin{bmatrix}
I_3 & 0_3 & 0_3 & 0_3 & 0_3 \\
0_3 & I_3 & 0_3 & 0_3 & 0_3 \\
0_3 & 0_3 & 0_3 & 0_3 & 0_3 \\
0_3 & 0_3 & 0_3 & 0_3 & 0_3 \\
0_3 & 0_3 & 0_3 & 0_3 & 0_3 \\
0_3 & 0_3 & \sqrt{\frac{2}{c_g s_t}}I_3 & 0_3 & 0_3 \\
0_3 & 0_3 & 0_3 & \sqrt{\frac{2}{c_a s_t}}I_3 & 0_3 \\
0_3 & 0_3 & 0_3 & 0_3 & \sqrt{\frac{2}{c_p s_t}}I_3
\end{bmatrix}
\begin{bmatrix}
[\boldsymbol{\alpha_e}]^{\boldsymbol{B}}_{\boldsymbol{IB}\,(k)} \\
\boldsymbol{\Delta a}^{\boldsymbol{B}}_{\boldsymbol{e}\,(k)} \\
\boldsymbol{\Delta b}^{\boldsymbol{B}}_{\boldsymbol{g}\,(k)} \\
\boldsymbol{\Delta b}^{\boldsymbol{B}}_{\boldsymbol{a}\,(k)} \\
\boldsymbol{\Delta b}^{\boldsymbol{E}}_{\boldsymbol{p}\,(k)}
\end{bmatrix}}_{\text{stochastic}}
\end{bmatrix}
\tag{6}
$$

$$
\begin{bmatrix}
[\boldsymbol{\omega_m}]^{\boldsymbol{B}}_{\boldsymbol{IB}\,(k)} \\
\boldsymbol{a}^{\boldsymbol{B}}_{\boldsymbol{m}\,(k)} \\
\boldsymbol{\delta\Psi}^{\boldsymbol{E}}_{\boldsymbol{m}\,(k)} \\
\boldsymbol{\delta v}^{\boldsymbol{E}}_{\boldsymbol{m}\,(k)} \\
\boldsymbol{\delta r}^{\boldsymbol{E}}_{\boldsymbol{m}\,(k)}
\end{bmatrix}
=
\begin{bmatrix}
I_3 & 0_3 & 0_3 & 0_3 & 0_3 & I_3 & 0_3 & 0_3 \\
0_3 & I_3 & 0_3 & 0_3 & 0_3 & 0_3 & I_3 & 0_3 \\
0_3 & 0_3 & I_3 & 0_3 & 0_3 & 0_3 & 0_3 & 0_3 \\
0_3 & 0_3 & 0_3 & I_3 & 0_3 & 0_3 & 0_3 & 0_3 \\
0_3 & 0_3 & 0_3 & 0_3 & I_3 & 0_3 & 0_3 & I_3
\end{bmatrix}
\begin{bmatrix}
[\boldsymbol{\omega_e}]^{\boldsymbol{B}}_{\boldsymbol{IB}\,(k)} \\
\boldsymbol{a}^{\boldsymbol{B}}_{\boldsymbol{e}\,(k)} \\
\boldsymbol{\delta\Psi}^{\boldsymbol{E}}_{\boldsymbol{e}\,(k)} \\
\boldsymbol{\delta v}^{\boldsymbol{E}}_{\boldsymbol{e}\,(k)} \\
\boldsymbol{\delta r}^{\boldsymbol{E}}_{\boldsymbol{e}\,(k)} \\
\boldsymbol{b}^{\boldsymbol{B}}_{\boldsymbol{g}\,(k)} \\
\boldsymbol{b}^{\boldsymbol{B}}_{\boldsymbol{a}\,(k)} \\
\boldsymbol{b}^{\boldsymbol{E}}_{\boldsymbol{p}\,(k)}
\end{bmatrix}
+
\begin{bmatrix}
[\boldsymbol{\Delta\omega_m}]^{\boldsymbol{B}}_{\boldsymbol{IB}\,(k)} \\
\boldsymbol{\Delta a}^{\boldsymbol{B}}_{\boldsymbol{m}\,(k)} \\
\boldsymbol{\Delta\Psi}^{\boldsymbol{E}}_{\boldsymbol{m}\,(k)} \\
\boldsymbol{\Delta v}^{\boldsymbol{E}}_{\boldsymbol{m}\,(k)} \\
\boldsymbol{\Delta r}^{\boldsymbol{E}}_{\boldsymbol{m}\,(k)}
\end{bmatrix}
$$

where 0_i is a $i \times i$ zero matrix. The vectors $[\boldsymbol{\alpha_e}]^{\boldsymbol{B}}_{\boldsymbol{IB}}$ and $\boldsymbol{\Delta a}^{\boldsymbol{B}}_{\boldsymbol{e}}$ represent the angular acceleration and jerk estimations. The measurements of the gyroscope $[\boldsymbol{\omega_m}]^{\boldsymbol{B}}_{\boldsymbol{IB}}$ and accelerometer $\boldsymbol{a}^{\boldsymbol{B}}_{\boldsymbol{m}}$ are affected by the corresponding noises ($[\boldsymbol{\Delta\omega_m}]^{\boldsymbol{B}}_{\boldsymbol{IB}}$, $\boldsymbol{\Delta a}^{\boldsymbol{B}}_{\boldsymbol{m}}$). The rotation matrix from the body to the navigation frame is $\mathbf{T}^{\mathbf{E}}_{\mathbf{B}}$ and the Earth rate is $\boldsymbol{\omega}^{\boldsymbol{E}}_{\boldsymbol{IE}}$. The superscripts $\{\cdot\}^E$ and $\{\cdot\}^B$ indicate that the variable is represented in the Earth frame and the body frame, respectively.

Using the compact version of equation (6):

$$
\boldsymbol{x}_{(k+1)} = A_k \boldsymbol{x}_{(k)} + B_{m_{(k)}} \boldsymbol{u}_{\boldsymbol{m}\,(k)} + B_{s(k)} \boldsymbol{u}_{\boldsymbol{s}\,(k)}
$$

the state covariance matrix Q is:

$$
Q_{(k)} = B_{s(k)} Q_{s(k)} B^T_{s(k)}
$$

where:

$$
Q_{s(k)} = \begin{bmatrix}
E\left[[\boldsymbol{\alpha_e}]^{\boldsymbol{B}}_{\boldsymbol{IB}\,(k)} [\boldsymbol{\alpha_e}]^{\boldsymbol{B}\,T}_{\boldsymbol{IB}\,(k)}\right] & 0_3 & 0_3 & 0_3 & 0_3 \\
0_3 & E\left[\boldsymbol{\Delta a}^{\boldsymbol{B}}_{\boldsymbol{e}\,(k)} \boldsymbol{\Delta a}^{\boldsymbol{B}\,T}_{\boldsymbol{e}\,(k)}\right] & 0_3 & 0_3 & 0_3 \\
0_3 & 0_3 & E\left[\boldsymbol{\Delta b}^{\boldsymbol{B}}_{\boldsymbol{g}\,(k)} \boldsymbol{\Delta b}^{\boldsymbol{B}\,T}_{\boldsymbol{g}\,(k)}\right] & 0_3 & 0_3 \\
0_3 & 0_3 & 0_3 & E\left[\boldsymbol{\Delta b}^{\boldsymbol{B}}_{\boldsymbol{a}\,(k)} \boldsymbol{\Delta b}^{\boldsymbol{B}\,T}_{\boldsymbol{a}\,(k)}\right] & 0_3 \\
0_3 & 0_3 & 0_3 & 0_3 & E\left[\boldsymbol{\Delta b}^{\boldsymbol{E}}_{\boldsymbol{p}\,(k)} \boldsymbol{\Delta b}^{\boldsymbol{E}\,T}_{\boldsymbol{p}\,(k)}\right]
\end{bmatrix}
$$

and the observation covariance matrix R is:

$$R_{(k)} = \begin{bmatrix} E\left[[\boldsymbol{\Delta\omega_m}]^{\boldsymbol{B}}_{\boldsymbol{IB}(k)}[\boldsymbol{\Delta\omega_m}]^{\boldsymbol{B}\,T}_{\boldsymbol{IB}(k)}\right] & 0_3 & 0_3 & 0_3 & 0_3 \\ 0_3 & E\left[\boldsymbol{\Delta a}^{\boldsymbol{B}}_{\boldsymbol{m}(k)}\boldsymbol{\Delta a}^{\boldsymbol{B}\,T}_{\boldsymbol{m}(k)}\right] & 0_3 & 0_3 & 0_3 \\ 0_3 & 0_3 & E\left[\boldsymbol{\Delta\Psi}^{\boldsymbol{E}}_{\boldsymbol{m}(k)}\boldsymbol{\Delta\Psi}^{\boldsymbol{E}\,T}_{\boldsymbol{m}(k)}\right] & 0_3 & 0_3 \\ 0_3 & 0_3 & 0_3 & E\left[\boldsymbol{\Delta v}^{\boldsymbol{E}}_{\boldsymbol{m}(k)}\boldsymbol{\Delta v}^{\boldsymbol{E}\,T}_{\boldsymbol{m}(k)}\right] & 0_3 \\ 0_3 & 0_3 & 0_3 & 0_3 & E\left[\boldsymbol{\Delta r}^{\boldsymbol{E}}_{\boldsymbol{m}(k)}\boldsymbol{\Delta r}^{\boldsymbol{E}\,T}_{\boldsymbol{m}(k)}\right] \end{bmatrix}$$

2.3 Angular acceleration and jerk variances modelling

In order to include the launcher dynamics knowledge, $E\left[[\boldsymbol{\alpha_e}]^{\boldsymbol{B}}_{\boldsymbol{IB}(k)}[\boldsymbol{\alpha_e}]^{\boldsymbol{B}\,T}_{\boldsymbol{IB}(k)}\right]$ and $E\left[\boldsymbol{\Delta a}^{\boldsymbol{B}}_{\boldsymbol{e}\,(k)}\boldsymbol{\Delta a}^{\boldsymbol{B}^T}_{\boldsymbol{e}\,(k)}\right]$ must be adjusted throughout the mission. The goal is to approximate an envelope of the angular acceleration and jerk amplitudes. Base on a priori knowledge of the forces acting on the launcher, heuristic models of the jerk and angular acceleration standard deviations are developed.

The trajectory of a satellite launcher is mostly directed toward one direction. Therefore, the variations of the angular velocity and acceleration are slow and can be considered almost null all through the mission. The only exceptions are during stage separations and direction changes (e.g. kick turn maneuver); however these are known events. An important unknown is the effect of the wind. During the coast phase, lateral thrusters are used to maintain the desired launcher attitude, which could slightly affect the angular velocity and acceleration of the launcher. However, no attitude changes are commanded during the coast phase. Therefore, the lateral thruster effects are not significant and are considered as unknown.

2.3.1 Angular acceleration variance modelling

The attitude of the launcher in the body roll axis is maintained constant during the whole mission and is barely perturbed by external forces. Therefore, the angular acceleration in the roll axis $[\alpha_{e\phi}]^B_{IB}$ is considered as being affected only by unknown forces and its standard deviation model is:

$$\text{std}\left([\alpha_{e\phi}]^B_{IB(k)}\right) rad/s^2 = 0.002$$

The standard deviation models for the pitch $[\alpha_{e\theta}]^B_{IB}$ and yaw $[\alpha_{e\psi}]^B_{IB}$ angular accelerations are:

$$\text{std}\left([\alpha_{e\theta}]^B_{IB(k)}\right) rad/s^2 = \left|\frac{5}{2s+1}\left([\alpha_{c\theta}]^B_{IB(k)}\right)\right| + \begin{cases} 0.002, & \text{if coast phase} \\ 0.02, & \text{if boost phase} \end{cases} \tag{7}$$

$$\text{std}\left([\alpha_{e\psi}]^B_{IB(k)}\right) rad/s^2 = \left|\frac{5}{2s+1}\left([\alpha_{c\psi}]^B_{IB(k)}\right)\right| + \begin{cases} 0.002, & \text{if coast phase} \\ 0.02, & \text{if boost phase} \end{cases} \tag{8}$$

where $[\alpha_{c\theta}]^B_{IB}$ and $[\alpha_{c\psi}]^B_{IB}$ are respectively the commanded angular accelerations in the body pitch and yaw axes. These are calculated using the second derivative (approximated by finite difference) of the commanded attitude. The choice of exploiting the guidance algorithm commands instead of the thrust nozzle orientations is motivated by the fact that the latter is highly affected by the angular velocity estimation error. Therefore, relying on the nozzle orientations makes the modelled angular acceleration standard deviation to grow rapidly to a point where the angular dynamics is considered as completely unknown. The time constant of the filter is based on the time required for the launcher to complete a turn maneuver and the gain is chosen to represent the maximum angular acceleration amplitude. The second term on the right end side of equations (7) and (8) represents the unknown forces. During the coast phase, the pitch and yaw are maintained constant and external forces have little effect of the launcher. However, during boost phases the attitude can be affected by the wind or by thrust nozzle movements.

2.3.2 Jerk variance modelling

The x-axis acceleration varies slowly during boost phases, is almost constant during the coast phase and changes rapidly during motor firing and separation events. Turn maneuvers have little impact on the x-axis jerk $\Delta a_{e_x}^B$. Therefore, the x-axis jerk standard deviation is modelled as follows:

$$\text{std}\left(\Delta a_{e_x}^B{}_{(k)}\right) m/s^3 = \begin{cases} 10, & \text{if coast phase} \\ 15, & \text{if boost phase} \\ 15000, & \text{if phase is changing} \end{cases}$$

Engine startup time can range from a few milliseconds to a few seconds and the power may decrease during the later portion of the motor tail-off [22, 23]. In the simulator exploited for this research, motors are modelled as perfect (instantaneous firing and no loss of power during tail-off) and stage separations do not affect the trajectory of the launcher. However, to get a more realistic mission scenario, the navigation function considers the stage separations and motor firing sequences as lasting three seconds, one second before they occur and two seconds afterwards.

Unlike the angular velocity, which is used by the launcher control function, the acceleration is not directly exploited by the guidance and control functions of the launcher. Therefore, the acceleration estimation error does not have a direct impact on the thrust nozzle orientation. However, the movement of the thrust nozzle is directly impacting the lateral acceleration. Therefore, the models used to capture jerks with greater amplitude during maneuvers are based on the commanded thrust nozzle orientation and dynamics. The standard deviation models for the y-axis $\Delta a_{e_y}^B$ and z-axis $\Delta a_{e_z}^B$ lateral jerks are:

$$\text{std}\left(\Delta a_{e_y}^B{}_{(k)}\right) m/s^3 = \left| \frac{30}{0.035s+1} \left(\Delta \xi_{c\psi(k)}^B\right) \right| + 10 \tag{9}$$

$$\text{std}\left(\Delta a_{e_z}^B{}_{(k)}\right) m/s^3 = \left| \frac{30}{0.035s+1} \left(\Delta \xi_{c\theta(k)}^B\right) \right| + 10 \tag{10}$$

where $\Delta\xi_{c\psi}$ and $\Delta\xi_{c\theta}$ are the variations of the commanded thrust nozzle angles (in rad/s) to correct respectively the yaw and pitch of the launcher. The variations of the thrust nozzle angles are obtained using the derivative of the commanded nozzle angles (approximated by finite difference). The time constant of the filter corresponds to the dynamics of the thrust nozzle movement and the gain of the filter represents the proportionality ratio between the lateral acceleration and the nozzle orientation change. The second term on the right end side of equations (9) and (10) capture the effects of the unknown forces (wind, lateral thruster, etc.)

2.4 Navigtation performance analysis

This section analyzes the performances of the navigation solution with a simplified stochastic model of the launcher knowledge. Many navigation solutions presented in the introduction (section 1) suffer from observability problems unless some maneuvers are done. If those maneuvers are not possible, as with a satellite launcher, the navigation solution may diverge. To ensure navigation stability, the observability of the new navigation model is verified using the observability matrix. Then, the proper evaluation of the angular acceleration and jerk standard deviations by the corresponding heuristic model is validated. The next test verifies that considering the dynamics of the launcher as unknown does not degrade the performances in comparison to the baseline navigation solution. Finally, the navigation with the launcher dynamics is compared to the baseline navigation system and the theoretical results are confirmed by Monte-Carlo simulations. The time evolution of the estimate standard deviations are used as comparisons basis. Section 2.4.1 presents the simulation parameters and section 2.4.2 analyzes the results.

2.4.1 Simulation parameters

The simulated mission is intended to put a satellite on a circular sun-synchronous orbit at an altitude of 500 km. The launch is performed from Churchill, Manitoba in Canada. The endoatmospheric phase guidance is

done in open loop (i.e. the attitude set points, computed before launch, are not updated in flight) and the exoatmospheric phase guidance is done using the Schuller estimation [14, 24]. The exoatmospheric phase begins when the thermal flux falls below a predetermined tolerance threshold which allows dropping the thermal protection fairing [14]. Three motors are used, two are fired before the coast phase and one is fired during the final phase. Figure 1 summarizes the mission phase timeline. The sampling rate of the simulation is 200 Hz and each Monte-Carlo simulation includes 20 launches.

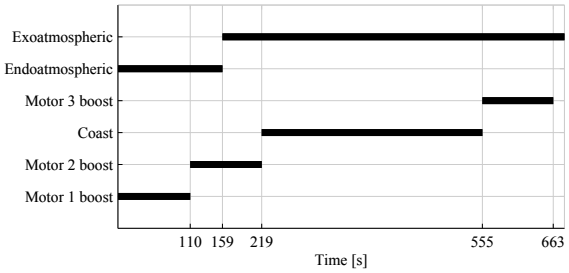

Figure 1: Mission phase timeline.

The sensor specifications are given in table 1. The INS specifications are inspired by the IMU-KVH1750 unit from Novatel®. The sampling rate is 1Hz for the GPS and attitude reference sensors and 200Hz for the accelerometers and gyroscopes.

Table 1: Sensors specifications

GPS receiver	C/A code with wide correlator
Gyroscope radom walk	$0.72°/h/\sqrt{Hz}$
Gyroscope bias stability	$0.05°/h$
Accelerometer radom walk	$117\mu g/\sqrt{Hz}$
Accelerometer bias stability	$7500\mu g$
Attitude reference sensor noise standard deviation	$1°$

2.4.2 Results analysis

The observability is verified by evaluating the rank of the observability matrix at each time step of the simulation. The rank of the observability matrix is 24 during the whole mission, which means that the proposed navigation solution does not introduce unobservable subspace to the baseline model [25]. This result was predictable since the six added states are directly observable with the gyroscope and accelerometer measurements.

To ensure the proper operation of the navigation filter, the angular acceleration and jerk must be within the standard deviations computed by the models presented in section 2.3. Figures 2 and 3 show the real angular acceleration in the pitch axis, the jerk in the z-axis and the corresponding computed standard deviations during the first 100 seconds of the mission. The effects of the kick turn maneuver and wind are identified and are within the modelled standard deviations.

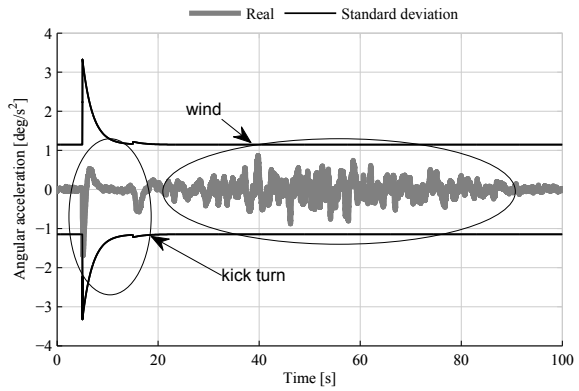

Figure 2: Real pitch angular acceleration versus modelled standard deviation.

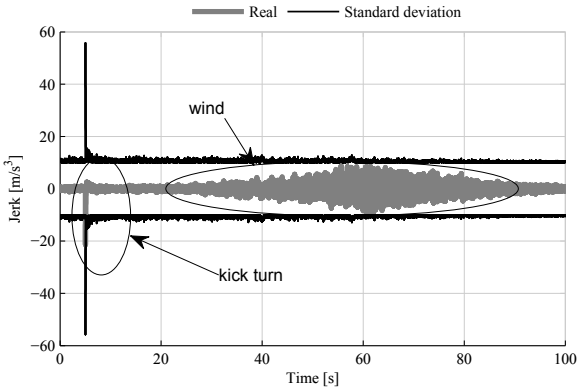

Figure 3: Real z-axis jerk versus modelled standard deviation.

As stated in section 2.2, if the jerk and angular acceleration are completely unknown and the corresponding variances set accordingly, the acceleration and angular velocity estimates rely almost completely on accelerometer and gyroscope measurements. The GPS and attitude reference sensors contribute to the acceleration and angular velocity estimation, but in a much lower proportion. Figure 4 shows the x-axis accelerometer measurements and the corresponding filtered values after firing the first engine. During the first 2 seconds, where the jerk is considered unknown, the filtered values match exactly the accelerometer measurements. This shows that considering the dynamics as unknown is equivalent to use the raw gyroscope and accelerometer measurements as in the baseline navigation system.

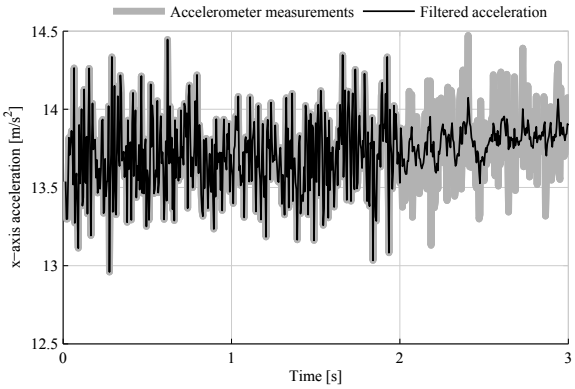

Figure 4: Raw x-axis accelerometer measurements versus filtered values after firing the first engine.

The inclusion of the angular velocity and acceleration into the navigation filter has an obvious impact on these estimates as shown in figures 5 and 6, where the estimation error standard deviations of the raw measurements and filtered values are compared. The real standard deviations from the Monte-Carlo simulation confirm the estimated standard deviations of the model which includes the angular velocity and acceleration estimations. The worst improvements are seen during the fast maneuvers. However, the estimates standard deviations do not exceed the results obtained with the baseline model. During the exoatmospheric boost phases, the trajectory of the launcher is updated by the guidance function, which generates many attitude correction maneuvers, thus limiting the potential angular velocity estimation gain in pitch and yaw axes. Obviously, the best improvements are obtained when the acceleration and angular velocity change slowly (table 2).

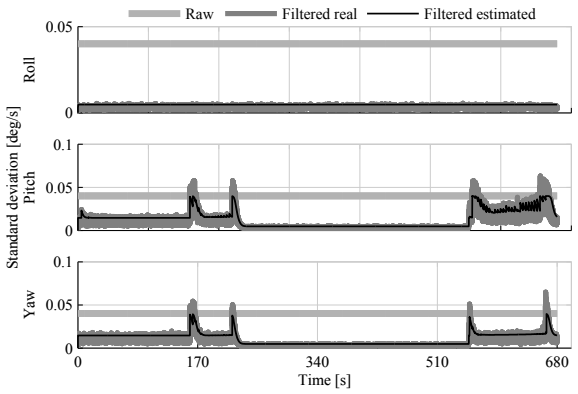

Figure 5: Comparison of the angular velocity estimation error standard deviations obtained with the raw gyroscope measurements and filtered values: real standard deviations from Monte-Carlo simulation and standard deviations estimated by the navigation filter.

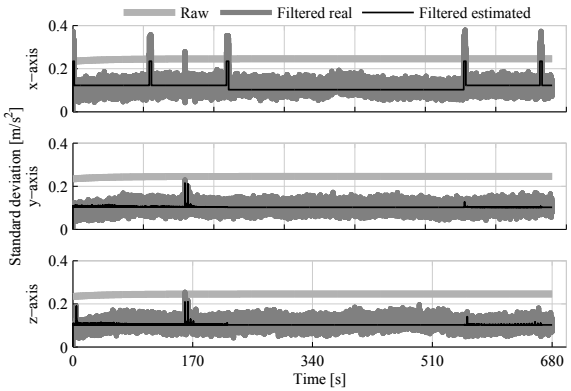

Figure 6: Comparison of the acceleration estimation error standard deviations obtained with the raw accelerometer measurements and filtered values: real standard deviations from Monte-Carlo simulations and standard deviations estimated by the navigation filter.

Table 2: Estimation improvements when the acceleration and angular velocity change slowly

		Boost phases	**Coast phase**
Angular velocity	**Roll**	88%	88%
	Pitch	64%	88%
	Yaw	64%	88%
Acceleration	**x-axis**	50%	58%
	y-axis	58%	58%
	z-axis	58%	58%

The other estimates are barely improved by the launcher dynamics knowledge, as it can be seen in figure 7 where the standard deviation of the roll estimation error is only reduced during the first seconds of the mission.

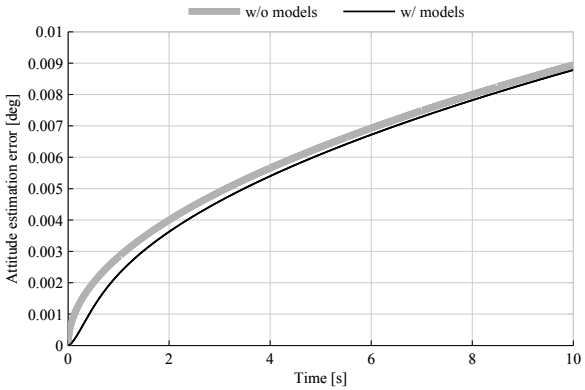

Figure 7: Comparison of the roll estimation error standard deviations with and without the stochastic model of the launcher

3 Control with filtered angular rate

The better angular velocity and acceleration estimation can be exploited, among other things, to improve fault detection and to refine the control function of the launcher. In the simulator used for this research, the control of the thrust nozzle orientation is done using the attitude and angular velocity. To illustrate the

advantage of the proposed approach, the filtered angular velocity is employed to reduce the amount of thrust nozzle movements. Less thrust nozzle movements reduces the on board total energy needed to operate them throughout the mission.

Two missions are simulated, one where the raw gyroscope measurements are used by the control function, and the other where the filtered angular velocity is employed. The two missions are done in the exact same conditions (i.e. wind, sensor noises, etc.). The total nozzle deflections to control the pitch and yaw, during the whole mission, are the comparison bases. These are obtained by the integrals of the nozzle movement absolute values in the corresponding axes.

Figure 8 shows an obvious reduction of the total nozzle movement when filtered angular velocity is used. The reduction at the end of the mission is 68% in the pitch axis and 70% in the yaw axis. The main improvements are during the first two boost phases, where the launcher trajectory is mainly affected by the wind and where the attitude change commands are limited. During the coast phase, the launcher attitude is controlled by lateral thrusters. Therefore, the thrust nozzle is not moved. During the last boost phase, the thrust nozzle movements are mostly due to commanded attitude changes which limit the gains.

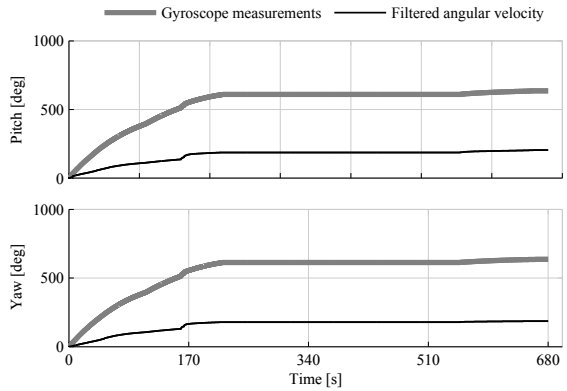

Figure 8: Comparison of the total thrust nozzle movements when the control function uses the raw gyroscope measurements versus the filtered angular velocities.

4 Conclusion

This paper proposed to use a simplified stochastic launcher model to improve the navigation performance. The model adds only six states to the navigation model, three for the angular velocity estimation and three for the acceleration estimation. The angular velocity and acceleration are modelled by random walks with known driving noise variances based on a priori knowledge of the launcher dynamics. The estimated values are then updated with the help of the gyroscope and accelerometer measurements.

The time evolution of the estimated standard deviations shows that the attitude, velocity and position estimates are barely improved. However, the angular velocity and acceleration estimation improvements are obvious. During fast attitude maneuvers, where the stochastic model is less effective, the performances are not degraded in comparison to the baseline navigation system. The rank of the observability matrix during the whole simulation confirms the observability of the proposed solution, even during the coast phase where the attitude maneuvers are limited.

The improved angular velocity estimation is then exploited by the control function. The results show that relying on the filtered angular velocity instead of the raw gyroscope measurements reduces the thrust nozzle movements significantly.

The application of the proposed solution is not limited to the angular velocity and acceleration estimates of a satellite launcher. This approach can be considered on any vehicles or processes where an estimated value varies slowly or when the estimated value change rate is within the estimation uncertainty.

References

[1] Y. Beaudoin, A. Desbiens, E. Gagnon, R. J. Landry, Improved satellite launcher navigation performance by using the reference trajectory data, in: Proceeding of International Navigation Conference 2015 (INC15), Royal Institute of Navigation, Manchester Conference Center, UK, 2015.

[2] S. Belin, J. F. Averlant, F. Dubuc, S. Villers, A. C. Reis, Requirements toward GNSS chain for ariane 5 mid-life evolution, in: 2010 5th ESA Workshop on Satellite Navigation Technologies and European Workshop on GNSS Signals and Signal Processing (NAVITEC), 2010, pp. 1–8. doi:10.1109/NAVITEC.2010.5708078.
URL http://dx.doi.org/10.1109/NAVITEC.2010.5708078

[3] M. Koifman, I. Y. Bar-Itzhack, Inertial navigation system aided by aircraft dynamics, IEEE Transactions on Control Systems Technology 7 (4) (1999) 487–493. doi:10.1109/87.772164.

[4] G. Dissanayake, S. Sukkarieh, E. Nebot, H. Durrant-Whyte, The aiding of a low-cost strapdown inertial measurement unit using vehicle model constraints for land vehicle applications, IEEE Transactions on Robotics and Automation 17 (5) (2001) 731–747. doi:10.1109/70.964672.

[5] M. Morgado, P. Oliveira, C. Silvestre, J. F. Vasconcelos, Embedded vehicle dynamics aiding for USBL/INS underwater navigation system, IEEE Transactions on Control Systems Technology 22 (1) (2014) 322–330. doi:10.1109/TCST.2013.2245133.

[6] M. Bryson, S. Sukkarieh, Vehicle model aided inertial navigation for a UAV using low-cost sensors, in: Australasian Conference on Robotics and Automation, 2004.

[7] M. Khaghani, J. Skaloud, Autonomous navigation of small UAVs based on vehicle dynamic model, in: International Archives of the Photogrammetry, Remote Sensing and Spatial Information Sciences - ISPRS Archives, Vol. 40, Lausanne, Switzerland, 2016, pp. 117 – 122, attitude accuracy;Autonomous navigation;Navigation accuracy;Navigation filters;Orders of magnitude;Proposed architectures;Satellite signals;Vehicle dynamic model;.
URL http://dx.doi.org/10.5194/isprsarchives-XL-3-W4-117-2016

[8] D. Vissière, P.-J. Bristeau, A. P. Martin, N. Petit, Experimental autonomous flight of a small-scaled helicopter using accurate dynamics model and low-cost sensors, in: Proceedings of the 17th World Congress The International Federation of Automatic Control, Vol. 41, Seoul, Korea, 2008, pp. 14642 – 14650. doi:http://dx.doi.org/10.3182/20080706-5-KR-1001.02480.
URL http://www.sciencedirect.com/science/article/pii/S1474667016413455

[9] P. Crocoll, J. Seibold, G. Scholz, G. F. Trommer, Model-aided navigation for a quadrotor helicopter: A novel navigation system and first experimental results, Navigation 61 (4) (2014) 253–271. doi:10.1002/navi.68.
URL http://dx.doi.org/10.1002/navi.68

[10] J. F. Vasconcelos, C. Silvestre, P. Oliveira, B. Guerreiro, Embedded UAV model and LASER aiding techniques for inertial navigation systems, Control Engineering Practice 18 (3) (2010) 262 – 278. doi:http://dx.doi.org/10.1016/j.conengprac.2009.11.004.
URL http://www.sciencedirect.com/science/article/pii/S0967066109002202

[11] X. Ma, S. Sukkarieh, K. J. H., Vehicle model aided inertial navigation, in: Intelligent Transportation Systems, 2003. Proceedings. 2003 IEEE, Vol. 2, 2003, pp. 1004–1009. doi:10.1109/ITSC.2003.1252637.

[12] J. B. Bancroft, Multiple IMU integration for vehicular navigation, in: 22nd International Technical Meeting of the Satellite Division of the Institute of Navigation 2009, ION GNSS 2009, Vol. 2, Savannah, GA, United states, 2009, pp. 1026 – 1038.

[13] D. Simon, Kalman filtering with state constraints: a survey of linear and nonlinear algorithms, IET Control Theory Applications 4 (8) (2010) 1303–1318. doi:10.1049/iet-cta.2009.0032.

[14] A. Vachon, Trajectographie d'un lanceur de satellites basée sur la commande prédictive, Ph.D. thesis, Université Laval, département de génie électrique et génie informatique, Québec, Canada (2012).

[15] L. D. Fairfax, F. E. Fresconi, Position estimation for projectiles using low-cost sensors and flight dynamics, Tech. rep., Army Research Laboratory (2012).

[16] S. J. Julier, H. F. Durrant-Whyte, On the role of process models in autonomous land vehicle navigation systems, IEEE Transactions on Robotics and Automation 19 (1) (2003) 1–14. doi:10.1109/TRA.2002.805661.

[17] O. J. Woodman, An introduction to inertial navigation, Tech. Rep. UCAM-CL-TR-696, University of Cambridge, Computer Laboratory (2007).

[18] M. Barczyk, M. Jost, D. R. Kastelan, A. F. Lynch, K. D. Listmann, An experimental validation of magnetometer integration into a GPS-aided helicopter UAV navigation system, in: American Control Conference (ACC), 2010, 2010, pp. 4439–4444. doi:10.1109/ACC.2010.5530999.

[19] Y. Zhao, M. Horemuz, L. E. Sjöberg, Stochastic modelling and analysis of imu sensor errors, Archives of Photogrammetry, Cartography and Remote Sensing 22 (2011) 437–449.

[20] M. Wis, I. Colomina, Dynamic dependent IMU stochastic modeling for enhanced INS/GNSS navigation, in: 2010 5th ESA Workshop on Satellite Navigation Technologies and European Workshop on GNSS Signals and Signal Processing (NAVITEC), 2010, pp. 1–5. doi:10.1109/NAVITEC.2010.5708041.

[21] H. Chang, L. Xue, W. Qin, G. Yuan, W. Yuan, An integrated MEMS gyroscope array with higher accuracy output, Sensors 8 (4) (2008) 2886–2899. doi:10.3390/s8042886.
URL http://www.mdpi.com/1424-8220/8/4/2886

[22] G. P. Sutton, O. Biblarz, Rocket Propulsion Elements, Wiley-lnterscience, 2001.

[23] D. Jeyakumar, K. K. Biswas, B. Nageswara Rao, Stage separation dynamic analysis of upper stage of a multistage launch vehicle using retro rockets, Mathematical and Computer Modelling 41 (8-9) (2005) 849 – 866.
URL http://dx.doi.org/10.1016/j.mcm.2005.02.001

[24] A. Vachon, E. Gagnon, A. Desbiens, C. Bérard, Guidage d'un lanceur de satellite basé sur l'approximation de Schuler, Tech. Rep. TM 2011-347, R&D pour la Défense Canada - Valcartier (2012).

[25] Y. Beaudoin, A. Desbiens, E. Gagnon, R. J. Landry, Observability of satellite launcher navigation with INS, GPS, attitude sensors and reference trajectory, Acta Astronautica 142 (2018) 277–288. doi:https://doi.org/10.1016/j.actaastro.2017.10.038.
URL https://www.sciencedirect.com/science/article/pii/S0094576517307002

DOCUMENT CONTROL DATA

*Security markings for the title, authors, abstract and keywords must be entered when the document is sensitive

1. ORIGINATOR (Name and address of the organization preparing the document. A DRDC Centre sponsoring a contractor's report, or tasking agency, is entered in Section 8.)

Canadian Aeronautics and Space Institute
350 Terry Fox Drive, Suite 104
Kanata, ON, K2K 2W5, Canada

2a. SECURITY MARKING (Overall security marking of the document including special supplemental markings if applicable.)

CAN UNCLASSIFIED

2b. CONTROLLED GOODS

NON-CONTROLLED GOODS
DMC A

3. TITLE (The document title and sub-title as indicated on the title page.)

Satellite launcher navigation aided by a stochastic model of the vehicle

4. AUTHORS (Last name, followed by initials – ranks, titles, etc., not to be used)

Beaudoin, Y.; Desbiens, A.; Gagnon, E.; Landry, René Jr.

5. DATE OF PUBLICATION (Month and year of publication of document.)	6a. NO. OF PAGES (Total pages, including Annexes, excluding DCD, covering and verso pages.)	6b. NO. OF REFS (Total references cited.)
June 2018	15	25

7. DOCUMENT CATEGORY (e.g., Scientific Report, Contract Report, Scientific Letter.)

External Literature (N)

8. SPONSORING CENTRE (The name and address of the department project office or laboratory sponsoring the research and development.)

DRDC - Valcartier Research Centre
Defence Research and Development Canada
2459 route de la Bravoure
Québec (Québec) G3J 1X5
Canada

9a. PROJECT OR GRANT NO. (If appropriate, the applicable research and development project or grant number under which the document was written. Please specify whether project or grant.)	9b. CONTRACT NO. (If appropriate, the applicable number under which the document was written.)
05ba - Space Situational Awareness	

10a. DRDC PUBLICATION NUMBER (The official document number by which the document is identified by the originating activity. This number must be unique to this document.)	10b. OTHER DOCUMENT NO(s). (Any other numbers which may be assigned this document either by the originator or by the sponsor.)
DRDC-RDDC-2018-N095	15eo

11a. FUTURE DISTRIBUTION WITHIN CANADA (Approval for further dissemination of the document. Security classification must also be considered.)

Public release

11b. FUTURE DISTRIBUTION OUTSIDE CANADA (Approval for further dissemination of the document. Security classification must also be considered.)

12. KEYWORDS, DESCRIPTORS or IDENTIFIERS (Use semi-colon as a delimiter.)

GPS (Global Positioning System); INS (Inertial Navigation System); Navigation; Vehicle Dynamics; Data Fusion

13. ABSTRACT/RÉSUMÉ (When available in the document, the French version of the abstract must be included here.)

The navigation system of a satellite launcher is of paramount importance. On a small launcher targeting low orbit, the navigation system may be a significant part of the total mission cost. A trend which is gaining interest is exploiting a model of the vehicle dynamics into the navigation system. Navigation with vehicle dynamics was evaluated on ground vehicles, aircrafts and unmanned helicopters/quadricopters. However, to the knowledge of the authors, navigation aided by the model of the dynamics has not been tested for satellite launchers.

Adding the vehicle dynamics knowledge into the navigation system can be as simple as adding non-holonomicity constraints or it may need a complete model of the vehicle dynamics. In this paper, a simple stochastic model that represents the angular velocity and acceleration as random walks with known driving noise variances, which are based on the vehicle dynamics, is exploited. The estimated values are then updated with the gyroscope and accelerometer measurements.

The results show that the attitude, velocity and position estimates are barely improved. However, the angular velocity and acceleration estimation errors are reduced significantly. Also, the proposed solution does not require special maneuvers to ensure the observability of the navigation model. To illustrate the advantage of the proposed approach, the improved angular velocity estimates are exploited in the control function instead of the raw gyroscope measurements to significantly reduce thrust nozzle movements.